Observational Evidence for Fast Mode Periodic Small-scale Shocks: A New Type of Plasma Phenomenon

Lican Shan[1,2] , Bruce T. Tsurutani[3], Yukiharu Ohsawa[4], Christian Mazelle[5], Can Huang[1,2] , Aimin Du[1,2,6,7],
Yasong S. Ge[1,2,6] , and Quanming Lu[8,9]

[1] Key Laboratory of Earth and Planetary Physics, Institute of Geology and Geophysics, Chinese Academy of Sciences, Beijing 100029, People's Republic of China;
lcshan@mail.iggcas.ac.cn, amdu@mail.iggcas.ac.cn
[2] Innovation Academy for Earth Science, CAS, Beijing 100029, People's Republic of China
[3] Jet Propulsion Laboratory, California Institute of Technology, Pasadena, California 91109, USA
[4] Department of Physics, Nagoya University, Nagoya 464-8602, Japan
[5] Institut de Recherche en Astrophysique et Planétologie, University Paul Sabatier, CNRS, Toulouse F-31400, France
[6] College of Earth and Planetary Sciences, University of Chinese Academy of Sciences, Beijing 100049, People's Republic of China
[7] Macau University of Science and Technology, Macau 999078, People's Republic of China
[8] CAS Key Lab of Geospace Environment, University of Science and Technology of China, Hefei 230026, People's Republic of China
[9] CAS Center for Excellence in Comparative Planetology, Hefei 230026, People's Republic of China

Abstract

We show observational evidence for a new form of collisionless shock in interplanetary space near Mars, small-scale shocks with periodic spacings. Pickup of new ionized hydrogen atoms in a magnetic field aligned with the solar wind direction causes the generation of a magnetosonic wave train through an ion beam instability. The waves have a frequency close to the local proton gyrofrequency. This is a similar physical process as for the formation of cometary plasma waves/turbulence. However, for the case of proton pickup near Mars, each individual magnetosonic wave cycle develops into a small-scale shock. So there is a string of fast mode shocks formed with proton gyroperiod spacings. These small-scale shocks display dissipation in the ions and dispersive whistlers. A fraction of ions trapped/reflected at the small-scale shocks are accelerated by the motional electric field. Observational results demonstrate that periodic shocks can perform the same functions as a single supercritical shock in a high-speed flow.

Unified Astronomy Thesaurus concepts: Interplanetary shocks (829); Planetary bow shocks (1246); Solar coronal mass ejection shocks (1997); Stellar bow shocks (1586)

1. Introduction

Newborn ions are created in interplanetary space (Zank 2015), at comets (Bavassano-Cattaneo et al. 1991), or upstream of planets with an exosphere (Yamauchi et al. 2015). The newborn ions are produced from neutral atoms via charge exchange with solar wind protons, solar photoionization, and/or electron impact ionization. As soon as the fresh ions are created, they can be picked up by the motional electric field of the solar wind. In cases where the solar wind flow speed is perpendicular to the interplanetary magnetic field (IMF), the motional electric field accelerates the newborn ions to form an energetic ring of ions (Wu & Davidson 1972). This ion distribution is unstable to the left-hand ion cyclotron instability (Kantrowitz & Petschek 1966; Glassmeier & Neubauer 1993; Mazelle et al. 1994; Tsurutani et al. 1995; Delva et al. 2008; Romanelli et al. 2016). The ion cyclotron waves pitch angle scatter the energetic ions, and then the ions become isotropic relative to the ambient magnetic field. However, when the IMF is parallel to the solar wind, there is no motional electric field to accelerate the ions. For this case of a pure ion beam flowing (at $-v_{sw}$ in the solar wind rest frame) through the solar wind plasma, a right-hand cyclotron resonant instability (Wu & Davidson 1972; Brinca 1991; Gary 1991) occurs and generates fast magnetosonic waves (Tsurutani & Smith 1986a, 1986b; Thorne & Tsurutani 1987).

For a magnetosonic wave propagating in the solar wind medium, the wave steepens due to the nonlinear interactions between the electromagnetic fields and the ions (Kantrowitz & Petschek 1966; Kennel & Sagdeev 1967; Hasegawa 1975). Previous observational study at comets (Tsurutani et al. 1987) and at Mars (Shan et al. 2020) unambiguously show that the magnetosonic wave amplitude grows and steepens, and finally forms periodic magnetic structures. However, to-date no one has shown that these steepened magnetosonic waves can actually form shocks.

Here we first report the direct evidence that photoionization of a hydrogen exosphere upstream of the Marian bow shock can lead to well-developed small-scale shocks with periodic spacings. Small-scale periodic shocks can perform the same functions of a single supercritical shock.

2. Data and Results

In this Letter we use magnetic field and plasma observations on 2016 December 24 using the MAVEN spacecraft. Figure 1 shows a 10 minute interval of the magnetic field (MAG; Connerney et al. 2015), ion number density and solar wind flow velocity (SWIA; Halekas et al. 2015), and electron temperature (SWEA; Mitchell et al. 2016). The ion density varies in-phase with the magnetic field magnitude and out-of-phase with the flow velocity, indicating that the waves are in the magnetosonic branch. The average duration of the adjacent leading-edges is about 36 ± 3 s in the spacecraft frame, comparable to the local proton gyroperiod (34 ± 2 s) in the unshocked solar wind. These values strongly indicate that the periodic shocks are essentially determined by the newborn proton gyromotion (see the Appendix).
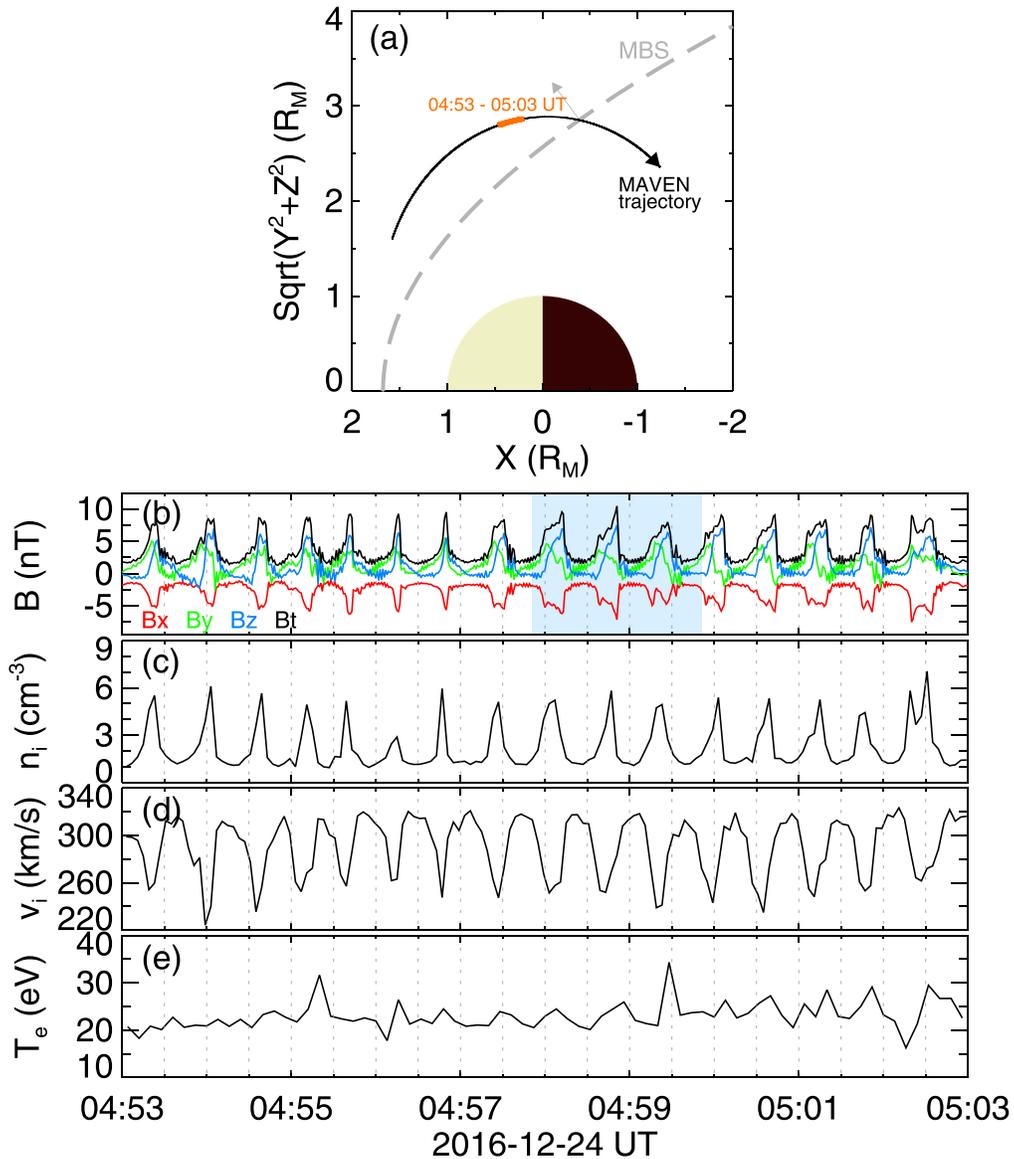
Figure 1. Overview of a series of fast mode structures by MAVEN spacecraft on 2016 December 24. Panel (a): MAVEN trajectory for the event. The dashed line represents a modeled bow shock for Mars (Vignes et al. 2000). Panel (b): magnetic field in the Mars-centered Solar Orbital (MSO) coordinate. Panels (c) and (d): ion number density and ion bulk velocity. Panel (e): electron temperature. The shaded time interval was used for Figure 2.

Figure 2 shows the magnetic field and ion differential energy fluxes (STATIC; McFadden et al. 2015) of the three steepened magnetosonic wave cycles. The gray, pink, green, and yellow shadings correspond to the selected upstream (unshocked), shock transition layer (STL; including magnetic ramps in the present event), foot and downstream (shocked) regions of periodic shocks, respectively. The magnetic fields in Figure 2(a) are shown in the shock coordinate system (SFC). The frame is determined by the shock normal and the direction of the maximum magnetic field (corresponding to the magnetic vector " $\boldsymbol{B_m}$ " at the position X_m) near the shock ramps. The x-axis is along the normal to each shock. In the plane x-$\boldsymbol{B_m}$, the z-axis is parallel to the magnetic field component perpendicular to the x-axis. The y-axis completes the right-handed coordinate system. In the SCF system, the B_y field component generated by the shock wave is proportional to $\partial B_z/\partial x$, and B_z has a profile similar to the plasma density, the electric potential, and the transverse electric field E_y (Ohsawa 2014). The magnetic structures ahead of (behind) each shock ramp appear to be

"feet" (overshoots) although the periodic shocks have only a moderate shock normal angle (angles of the shock normals relative to the unshocked, upstream magnetic fields). The shock normal angles are presented in Table 1.

The ratios of the fast magnetosonic Mach number to the critical Mach number (M_f/M_c) for the three shocks are ~1.9, ~1.6, and ~1.5 (see Edmiston & Kennel 1984), respectively. The values indicate that they are weak, supercritical shocks. High-frequency whistler precursors are observed usually in front of a supercritical shock front (Sundkvist et al. 2012; Wilson et al. 2012). As the fast magnetosonic Mach number is less than the whistler critical Mach number ($M_w = \frac{1}{2}\cos\theta_{Bn}$ $\sqrt{\frac{m_p}{m_e}}$, m_p and m_e are the proton and electron mass, respectively), e.g., $M_f/M_w < 1$ (~0.12 in the present study) for all three cases shown, the linear whistler in the present study should almost phase-stand with respect to the shock front (Kennel et al. 1985). The dispersive whistler waves are responsible for releasing energy from a stationary shock to prevent further
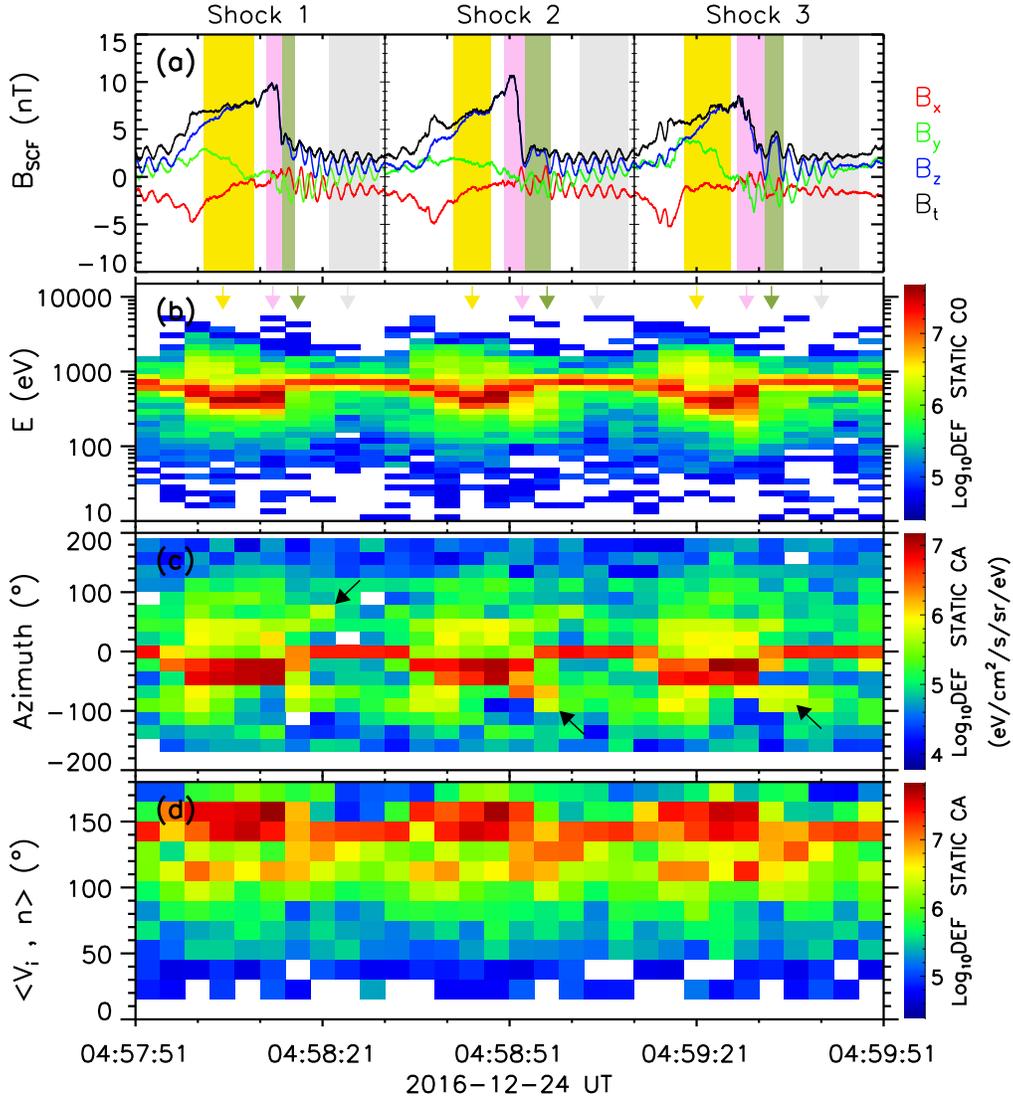
Figure 2. Characteristics of three well-developed periodic shocks in magnetic field and ion energy flux profiles. (a) High-time-resolution (32 sample s^{-1}) magnetic field in the SCF. (b)–(d) Differential energy flux of ions as a function of (b) energy, (c) azimuth of the instrument, and (d) the angle between ion velocities and the shock normal, respectively. The color-coded arrows in Figure 2(b) show the location of the cuts presented in Figure 3.

steepening, especially as the wavelength approaches the dissipation scale that should be required to be shorter than the STL (Treumann 2009).

Figure 2(b) shows the ion energy fluxes as a function of energy. The central energy of the unshocked ion flow is $\sim$720 eV. It is clear that most ions are decelerated as they pass through the shock ramps. Simultaneously, the solar wind ions should also be thermalized downstream through irreversible shock heating that corresponds to the ion entropy increase. Figure 2(c) shows the ion energy fluxes as a function of azimuth angle in the instrument frame. The unshocked ions are centered at $\sim$0°, while the shocked ions have a much broader azimuth angle range. It should be noted that some ion fluxes (marked by black arrows in Figure 2(c)), upstream and close to the shock ramps, have different azimuth angles from the unshocked ions. The unshocked ion beam has a small inclination from the background magnetic field upstream (similar to the angle θ_{Bx} in Table 1), while the ions indicated by black arrows are quasi-perpendicular to the field (not shown here). Those ions marked by arrows in Figure 2(c) may be trapped and reflected (or scattered) by the shock

electromagnetic fields, which are also displayed in the distributions in Figure 3. Figure 2(d) displays the angular (angles between the ion velocities and shock normal) distributions of the ions. The inflowing ions are injected at a moderate angle (fixed at $\sim$140°) into the shocks. By contrast, the shocked ions exhibit a diffusive distribution that is dominated by two populations. One ion population (angular range approximately from $\sim$135° to 165°) is the decelerated bulk flow ions. The other population with angle $\sim$110° represents the accelerated ions (higher-energy components of yellow lines in Figure 3).

Figure 3 shows the distributions of the normalized ion energy fluxes in the upstream (Ups.), foot, STL, and downstream (Dow.) regions of the three periodic shocks. It should come as no surprised that the unshocked ions (gray lines) with energy $\sim$720 eV are heated and decelerated (see the pink lines) as the ions encounter the shocks. Interestingly, two small fractions of ion populations, e.g., lower-energy ($<\sim$500 eV) and higher-energy ($>\sim$1 keV) ions, are identified at the shock feet (green lines) although the average kinetic energy of the bulk of the plasma is still at a value of $\sim$720 eV for the flow

Table 1
Periodic Shocks and Plasma Parameters

Parameter	Value		
	Shock 1	Shock 2	Shock 3
Unshocked magnetic field $\boldsymbol{B}$ (nT)[a]	[−1.63, 0.89, −0.04]	[−1.73, 1.00, 0.05]	[−1.78, 0.88, 0.09]
Unshocked magnetic field angle θ_{Bx} (°)	29	30	26
Unshocked ion flow velocity $\boldsymbol{V}$ (km/s)	[−308.3, 58.0, 3.7]	[−310.3, 64.7, 6.3]	[−299.4, 65.7, 17.0]
Unshocked ion density (cm^{-3})	1.17	1.20	1.29
Unshocked electron inertial length λ_e (km)	4.4	4.5	4.7
Unshocked proton convective gyroradius r_{ci} (km)	1763	1655	1612
Compression ratio of magnetic field	3.9	3.3	3.2
Shock normal $\boldsymbol{n}$[b]	[0.69, −0.29, 0.67]	[0.69, −0.37, 0.63]	[0.85, −0.11, 0.51]
	[0.77, −0.10, 0.63]	[0.80, −0.11, 0.59]	[0.88, −0.17, 0.45]
Shock angle θ_{Bn} (°)	41	40	33
	43	43	33
Shock speed V_{sh} (km/s)[c]	170	155	161
Width of the steepest magnetic part of the ramp L_r (λ_e)	12.9	21.8	23.4
Wavelength L_w (λ_e)[d]	42.5	49.2	60.0
Alfvén Mach number M_A	4.6	3.9	4.2
Magnetosonic Mach number M_f[e]	2.2	1.9	2.0
M_f/M_c	∼1.9	∼1.6	∼1.5

Notes.

[a] All vectors are in the MSO coordinate system.

[b] n is the shock normal direction calculated with the magnetic field coplanarity and Abraham-Schrauner (Abraham-Shrauner 1972) methods, respectively. Except for the cases where shock normal angles are determined by both methods, other parameters associated with the normal are computed with the former method.

[c] V_{sh} is the shock velocity in the solar wind rest frame. The calculation is based on the assumption of the mass flux conservation (Tsurutani & Lin 1985).

[d] L_w is the relative wavelength $\left(=2\pi\lambda_e \cos\theta_{Bn}\sqrt{\frac{m_p}{m_e}}/M_A\right)$ of whistler in the limiting case of phase standing upstream (Schwartz et al. 2011).

[e] Because of the limitation of on-board-computed ion temperature (Halekas et al. 2017), we use an assumption that the ion temperature is one-third of electron temperature (Liu et al. 2005).

energy. The higher-energy ions have been trapped at the shock feet and were accelerated by the convection electric field upstream. Furthermore, if the higher-energy component (>∼1 keV) of the ion distribution downstream (yellow lines) consists of those accelerated ions, a multiple-acceleration process may be necessary (Burgess & Schwartz 1984). The average of the bulk kinetic energy decreases from ∼720 eV to 410 eV as the ions pass through the shocks. Note that the ion flows appear to slow down further in the downstream regions after they are partially retarded at the shock ramps. This may be the result of the spatial (quasi-adiabatic) expansion of the downstream regions.

3. Conclusions and Discussion

We report a new type of collisionless fast mode shock wave in this Letter. The results stress that the periodic shocks can perform the same functions of a solitary supercritical shock standing in front of a planetary magnetosphere within the heliosphere. Energy redistribution takes place at the small shocks through both dissipation and dispersion. A portion of incident ions are trapped and reflected, and then accelerated by the motional electric field.

The energy transformation by anomalous resistivity (heating and diffusion through wave-particle interactions) is critical for the balance between nonlinearity and dissipation to sustain a low Mach shock (Kennel et al. 1985). For a supercritical shock, since thermalization could not generate sufficient dissipation, the emergence of a small fraction of backstreaming ions is an efficient way to maintain the shock steepening (Edmiston & Kennel 1984). The Mars exosphere can extend beyond the Martian bow shock. A previous study has shown that the

newborn ions can contribute ∼1% to the solar wind density at the positions close to the Martian bow shock (Dubinin et al. 2006). The observed solar wind and downstream ions may be mixed with some newborn ions. Those pickup ions can also be accelerated and heated effectively at the shock front (Zank et al. 1996; Zirnstein et al. 2018; Lembége et al. 2020). In light of the specific frequencies noted in the observations, the well-developed periodic shocks are suggested to evolve from a fast magnetosonic wave train that was excited by newborn protons beaming in the antisolar wind direction, which can be sketched in Figure 4.

Future work will investigate the interactions of periodic shock fields with charged particles and conduct an analysis on the particle acceleration process at the shocks. It appears possible that reflected ions can be energized by Fermi acceleration especially as the space scale varies between two adjacent periodic shock fronts. Efforts from theoretical and Particle-In-Cell (PIC) simulation research will be performed to better understand the microphysical processes that are taking place.
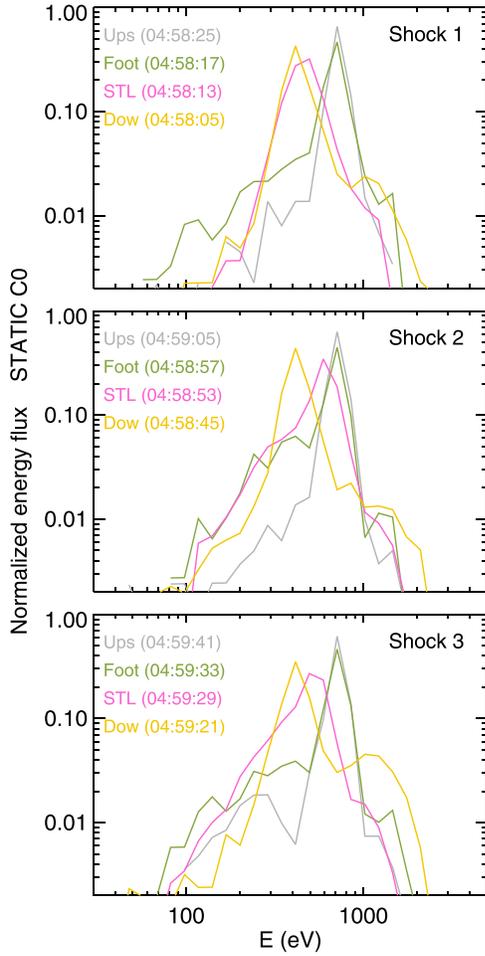
Figure 3. Normalized distribution of ion energy fluxes for the three shocks. The lines represent the distributions for upstream (gray), foot (green), STL (pink), and downstream (yellow) ions, respectively.

Appendix
The Observed Frequency of the Wave Excited by a Quasi-parallel Newborn Ion Beam

As the newborn ions are created by photoionization, charge exchange, and/or electron impact ionization, they are at rest in the spacecraft frame but have a speed $-v_{sw}$ relative to the solar wind plasma. In cases where the solar wind velocity is quasi-parallel to the interplanetary magnetic field (IMF), a fast mode wave will be excited through a right-hand ion beam instability (Brinca 1991) where the newborn ions form the beam. The wave frequency (ω) in the plasma rest frame satisfies the resonant condition:

$$\omega - \boldsymbol{k} \cdot \boldsymbol{v}_{//} = -n\Omega_i \quad (n\textbf{\color{red}?=?}1 \text{ for the fundamental frequency}), \quad (A1)$$

where $\boldsymbol{k}$ is the wavevector, $\Omega_i = qB/m$ (q and m are the charge and mass of the ion) is the ion gyrofrequency. $\boldsymbol{v}_{//}$ is the parallel speed of the newborn ions, which is about $-\boldsymbol{v}_{sw}$ for this situation. In view of the Doppler shift of the solar wind, the observed wave frequency (ω_{sc}) by the spacecraft is

$$\omega_{sc} = \omega + \boldsymbol{k} \cdot \boldsymbol{v}_{sw}. \quad (A2)$$

Combination of both Equation (A1) for the fundamental resonance and Equation (A2), we get the observed frequency of the wave,

$$\omega_{sc} \approx -\Omega_i. \quad (A3)$$

The minus sign represents that the wave is right-hand polarized in the plasma rest coordinates but left-handed polarization in the spacecraft frame (Mazelle & Neubauer 1993). This result indicates that the observed frequency of the wave excited by newborn ions is approximately the local ion gyrofrequency. In other words, the wave period in the spacecraft frame is essentially determined by the newborn ion gyromotion.

For a situation of a foreshock beam consisting of back-streaming ions through adiabatic reflection at a planetary bow shock, the ion velocity must be larger than ~$2v_{sw}$ in the solar wind rest frame to be able to travel upstream (Schwartz et al. 1983). Thus the observed frequency of the waves excited by the backstreaming ions through the right-hand ion beam instability should be much less than the local ion gyrofrequency. This argument indicates that the waves shown in Figure 1 cannot be generated by foreshock ions.
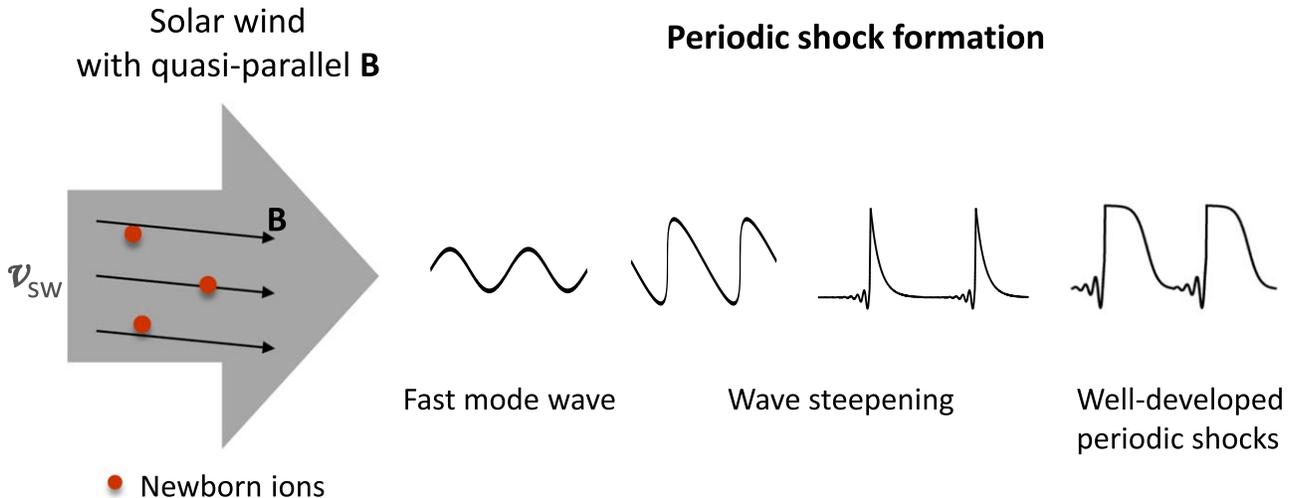

Figure 4. Schematics illustrating the well-developed periodic shock formation.

ORCID iDs

Lican Shan (ID) https://orcid.org/0000-0002-2354-9261
Can Huang (ID) https://orcid.org/0000-0003-0223-0494
Yasong S. Ge (ID) https://orcid.org/0000-0002-4345-522X
Quanming Lu (ID) https://orcid.org/0000-0003-3041-2682

References

Abraham-Shrauner, B. 1972, JGR, 77, 736
Bavassano-Cattaneo, M. B., Fonnisano, V., Amata, E., et al. 1991, in Comets in the Post Halley Era, ed. R. Newburn et al. (Noordwijk: ESA), 491
Brinca, A. 1991, GMS, 61, 211
Burgess, D., & Schwartz, S. J. 1984, JGR, 89, 7407
Connerney, J. E. P., Espley, J., Lawton, P., et al. 2015, SSRv, 195, 257
Delva, M., Zhang, T. L., Volwerk, M., et al. 2008, GeoRL, 35, L03105
Dubinin, E., Fraenz, M., Woch, J., et al. 2006, GeoRL, 33, L22103
Edmiston, J. P., & Kennel, C. F. 1984, JPlPh, 32, 429
Gary, S. P. 1991, SSRv, 56, 373
Glassmeier, K.-H., & Neubauer, F. M. 1993, JGR, 98, 20921
Halekas, J. S., Taylor, E. R., Dalton, G., et al. 2015, SSRv, 195, 125
Halekas, J. S., Ruhunusiri, S., Harada, Y., et al. 2017, JGRA, 122, 547
Hasegawa, A. 1975, Plasma Instabilities and Nonlinear Effects (Heidelberg: Springer)
Kantrowitz, A. R., & Petschek, H. E. 1966, Plasma Physics in Theory and Application (New York: McGraw-Hill)
Kennel, C. F., Edmiston, J. P., & Hada, T. 1985, GMS, 34, 1
Kennel, C. F., & Sagdeev, R. Z. 1967, JGR, 72, 3327
Lembége, B., Yang, Z., & Zank, G. P. 2020, ApJ, 890, 48

Liu, Y., Richardson, J. D., & Belcher, J. W. 2005, P&SS, 53, 3
Mazelle, C., & Neubauer, F. M. 1993, GeoRL, 20, 153
Mazelle, C., Reme, H., Neubauer, F. M., & Glassmeier, K.-H. 1994, AdSpR, 16, 41
McFadden, J. P., Kortmann, O., Curtis, D., et al. 2015, SSRv, 195, 199
Mitchell, D. L., Mazelle, C., Sauvaud, J.-A., et al. 2016, SSRv, 200, 495
Ohsawa, Y. 2014, PhR, 536, 147
Romanelli, N., Mazelle, C. X., Chaufray, J. Y., et al. 2016, JGRA, 121, 11113
Schwartz, S. J., Henley, E., Mitchell, J., & Krasnoselskikh, V. 2011, PhRvL, 107, 215002
Schwartz, S. T., Thomsen, M. F., & Gosling, J. T. 1983, JGR, 88, 2039
Shan, L., Du, A., Tsurutani, B. T., et al. 2020, ApJL, 888, L17
Sundkvist, D., Krasnoselskikh, V., Bale, S. D., et al. 2012, PhRvL, 108, 025002
Thorne, R. M., & Tsurutani, B. T. 1987, P&SS, 35, 1501
Treumann, R. A. 2009, A&Arv, 17, 409
Tsurutani, B. T., Glassmeier, K.-H., & Neubauer, F. M. 1995, GeoRL, 22, 1149
Tsurutani, B. T., & Lin, R. P. 1985, JGR, 90, 1
Tsurutani, B. T., & Smith, E. J. 1986a, GeoRL, 13, 259
Tsurutani, B. T., & Smith, E. J. 1986b, GeoRL, 13, 263
Tsurutani, B. T., Thorne, R. M., Smith, E. J., et al. 1987, JGR, 92, 11074
Vignes, D., Mazelle, C., Rème, H., et al. 2000, GeoRL, 27, 49
Wilson, L. B., III, Koval, A., Szabo, A., et al. 2012, GeoRL, 39, L08109
Wu, C. S., & Davidson, R. C. 1972, JGR, 77, 5399
Yamauchi, M., Hara, T., Lundin, R., et al. 2015, P&SS, 119, 54
Zank, G. P. 2015, ARA&A, 53, 449
Zank, G. P., Pauls, H. L., Cairns, I. H., & Webb, G. M. 1996, JGR, 101, 457
Zirnstein, E. J., McComas, D. J., Kumar, R., et al. 2018, PvRvL, 121, 075102